低下していた。臨床で1椎体をスライス厚2mmでCT撮像すると15～20スライスに相当し，組織荷重係数を0.2とすると放射線被曝量は3mSv程度となる。この被曝量は腰椎4方向のエックス線写真撮影の被曝量に相当するため，臨床応用可能と考えられた[6]。

本研究では，CT/有限要素法を用いて，閉経後女性における椎体骨折リスクおよび骨粗鬆症患者に対するアレンドロネートの効果を評価し，二重エネルギーエックス線吸収測定法(DXA：Lunar DPX-IQ)による骨密度(areal bone mineral density：aBMD)，CTによる骨密度(volumetric bone mineral density：vBMD)と比較・検討した。

1　対象と方法

1）閉経後女性における椎体骨折リスクの評価

骨代謝・骨強度に影響する既往歴・薬剤歴がなく，第2腰椎に骨折などの病変がない閉経後女性129人を対象として，倫理委員会の承認のもと対象者の書面による同意を得て行った。外傷性椎体骨折既往者を除外した104人[平均年齢71.3歳：椎体骨折なし(非骨折群)75人，非外傷性椎体骨折あり(骨折群)29人]に対してDXAにより第2～4腰椎のaBMDを，CTにより第2腰椎のvBMDを測定した。また，CT/有限要素法により第2腰椎の単軸圧縮強度である椎体強度値を解析し，CT/有限要素法が椎体骨折リスク評価に有用かを検討した。非外傷性椎体骨折をスクリーニングする椎体強度値をreceiver operating characteristic(ROC)解析により求めた。また，ロジスティック回帰分析(年齢・体重を補正)にて骨折リスクのオッズ比を求めた。

2）骨粗鬆症患者に対するアレンドロネート効果の評価

原発性骨粗鬆症の診断基準を満たし，骨代謝・骨強度に影響する既往歴・薬剤歴がなく，第2腰椎に骨折などの病変がない，アレンドロネート服用後に立位あるいは座位を30分以上保てる60歳以上の女性33人(平均年齢76.5歳)を対象とした。倫理委員会の承認のもと対象者の書面による同意を得て，5mg/日のアレンドロネートを投与した。DXAにより第2～4腰椎のaBMDをアレンドロネート投与開始前，および投与開始後6，12，18ヵ月時に測定した。第2腰椎のCTについては投与前，投与開始後3，6，12，18ヵ月時に撮影し，vBMDの測定およびCT/有限要素法による椎体強度値の解析を行った。また投与前および投与開始後3ヵ月時に尿中I型コラーゲン架橋N-テロペプチド(NTx)を測定した。

2　結　　果

1）椎体骨折リスクの評価[7]

対象者の閉経後女性104人のうち，非骨折群は平均年齢69.5±7.7歳(平均値±標準偏差)，平均身長150.6±5.1cm，平均体重51.5±7.3kgで，骨折群は平均年齢76.0±4.8歳，平均身長147.5±5.4cm，平均体重47.8±6.9kgであった。測定した平均aBMDは非骨折群が0.860±0.166g/cm^{2}で骨折群の0.719±0.209g/cm^{2}に比較して有意に大きく($p<0.05$：Mann-Whitney U検定)，平均vBMDは非骨折群が80.3±24.2mg/cm^{3}で骨折群の51.5±22.0mg/cm^{3}に比較して有意に大きく($p<0.0001$)，解析した平均椎体強度値は非骨折群が2.55±0.78kNで骨折群の1.59±0.51kNに比較して有意に高値を示した($p<0.0001$)。

ROC解析により検討した結果，非外傷性椎体骨折を効率よく判別できる至適カットオフ値は椎体強度値が1.95kNで体重の3.94倍の質量にかかる重量に相当し，感度75.9%・特異度78.7%であった。

対象者104人に対してロジスティック回帰分析にて年齢・体重を補正し骨折群の危険因子を評価したところ，1標準偏差の変化量に対するオッズ比はaBMDが1.83($p=0.0238$)，vBMDが3.57($p=0.0017$)，椎体強度値が6.71($p<0.0001$)と，椎体強度値の低下はaBMD・vBMDの低下より鋭敏な危険因子となっていた。椎体強度値のROC曲線下面積は0.822で，aBMD(面積0.713，$p=0.0010$)およびvBMD(面積0.767，

$p=0.0129$)より有意に高かった。

2) アレンドロネート効果の評価[7]

アレンドロネート投与開始前との変化率が追跡可能であったのは，投与期間12ヵ月までが33人，18ヵ月では6人であった。それぞれの平均変化率は，3ヵ月の椎体強度値が＋10.2%，6ヵ月が＋16.7%，aBMDでは＋3.7%，vBMDが＋5.1%，12ヵ月になると椎体強度値が＋26.9%，aBMDが＋7.5%，vBMDが＋8.8%であった。さらに，18ヵ月(6人)では椎体強度値が＋30.7%，aBMDが＋9.7%，vBMDが＋11.9%増加していた。

投与3ヵ月での椎体強度値変化率と尿中NTxの変化率は相関がなく($r=0.295$, $p=0.0955$)，投与12ヵ月での椎体強度値変化率とaBMD変化率には弱い相関($r=0.481$, $p=0.0046$)があった。CT/有限要素法による骨力学特性分析では，アレンドロネート投与前には圧縮ひずみが著しく骨折が生じやすいと考えられた領域において，投与後に圧縮ひずみの減少がみられた。また投与開始12ヵ月後には，椎体中央部の骨密度増加が8.3%($p=0.0013$)であったのに対し，皮質シェルを含む辺縁部では13.6%($p=0.0004$)の増加と，皮質近傍優位に薬剤効果がみられた。

3 考　　察

椎体骨折リスクの評価に関し，CT/有限要素法による椎体強度値はvBMDと同程度の識別能と報告されている[8]。一方，本研究では椎体強度値はaBMDおよびvBMDよりも有意に識別能が高かった。また，アレンドロネート効果の評価に関し，投与期間6ヵ月から18ヵ月のあいだでaBMDおよびvBMDは増加しているのに椎体強度値は減少したと報告されている[9]のに対し，本研究では投与期間18ヵ月においてaBMDおよびvBMDと同様ゆるやかではあるが，椎体強度値の増加が継続していた。

本研究が二つの先行研究と異なった結果である理由として，使用している有限要素モデルが異なることが一因と考えられる。先行研究では六面体要素であるのに対し，本研究は四面体要素を使用し，また本研究では先行研究にはない皮質シェルの構築を行っている。また，先行研究では延性材料に用いる理論および骨折定義を使用しているのに対し，本研究では引張に対しては脆性，圧縮に対しては弾塑性として，非線形解析にて降伏後の塑性も解析して骨の材料特性に基づき骨折の定義を行った点も，結果の相違に影響を与えたものと考える[5]。

アレンドロネートは投与開始後2～3年で骨密度の増加および新規骨折発生の抑制が得られることが報告されているが，臨床の場では投与開始後1年以内の，より早期に薬剤治療効果を知りたいという要求がある。本研究ではCT/有限要素法による椎体強度値はaBMD・vBMDより早期の投与開始後3ヵ月でアレンドロネートの効果判定に有用であった。また投与開始後18ヵ月間にわたり継続して椎体強度値の増加がみられた。

椎体強度値と尿中NTxの変化率に相関がないことより，椎体強度値は骨代謝を反映していないことが示唆された。一方，椎体強度値とaBMDの変化率には弱い相関があり，椎体強度値は骨密度を反映することが示唆された。またCT/有限要素法は骨密度に加え密度分布の変化を評価し，皮質近傍優位にアレンドロネート効果がみられていた。アレンドロネートの効果として皮質近傍の密度が増加するような密度分布の変化が生じ，圧縮応力の集中が軽減して圧縮ひずみ分布が改善し，椎体強度が増加したと考えられた。

アレンドロネートの皮質骨に対する効果としては，腸骨の微小血管造影法による評価でコントロール群と比較して石灰化度が皮質骨で9.3%，海綿骨で7.3%増加し，腸骨皮質骨で二次石灰化の延長があったと報告されている[10]。また腸骨の形態計測で，皮質骨中の多孔度が46%減少したと報告されている[11]。本研究では椎体において皮質シェル近傍優位に密度が増加していたが，骨微細構造について検討していない。腸骨皮質骨で報告されている二次石灰化の延長および多孔度の減少が椎体においても生じ

ているかについては，今後，組織学的検討，形態計測，マイクロCTなどによる評価が必要である。

また，骨リモデリングはマイクロダメージ，ひずみ，ひずみエネルギー密度に応答して生じるが，本研究ではアレンドロネートが圧縮ひずみやひずみエネルギー密度が大きい部位に直接作用しているわけではなく，皮質近傍の骨密度の増加により，結果として圧縮ひずみが軽減していた。アレンドロネートがどのパラメータに応答して作用するかは依然不明であり，今後の課題である。

骨粗鬆症診療におけるCT/有限要素法の役割として，骨強度を反映する要素のうち骨密度，密度分布，立体構造を評価できる点があげられるが，今後，CT/有限要素法とCT/有限要素法で評価できない骨代謝，骨微細構造の評価を組み合わせることにより，骨折リスク判定基準値の設定，骨粗鬆症治療薬剤効果の骨力学特性からの検証などに応用されることが期待される。

文　献

1) Keyak JH, Rossi SA, Jones KA, Skinner HB. Prediction of femoral fracture load using automated finite element modeling. J Biomech 1998;31:125-33.
2) Cody DD, Gross GJ, Hou FJ, Spencer HJ, Goldstein SA, Fyhrie DP. Femoral strength is better predicted by finite element models than QCT and DXA. J Biomech 1999;32:1013-20.
3) Silva MJ, Keaveny TM, Hayes WC. Computed tomography-based finite element analysis predicts failure loads and fracture patterns for vertebral sections. J Orthop Res 1998;16:300-8.
4) Crawford RP, Cann CE, Keaveny TM. Finite element models predict *in vitro* vertebral body compressive strength better than quantitative computed tomography. Bone 2003;33:744-50.
5) Imai K, Ohnishi I, Bessho M, Nakamura K. Nonlinear finite element model predicts vertebral bone strength and fracture site. Spine 2006;31:1789-94.
6) Imai K, Ohnishi I, Yamamoto S, Nakamura K. *In vivo* assessment of lumbar vertebral strength in elderly women using computed tomography-based nonlinear finite element model. Spine 2008;33:27-32.
7) Imai K, Ohnishi I, Matsumoto T, Yamamoto S, Nakamura K. Assessment of vertebral fracture risk and therapeutic effects of alendronate in postmenopausal women using a quantitative computed tomography-based nonlinear finite element method. Osteoporos Int 2009;20:801-10.
8) Melton LJ 3rd, Riggs BL, Keaveny TM, Achenbach SJ, Hoffmann PF, Camp JJ, et al. Structural determinants of vertebral fracture risk. J Bone Miner Res 2007;22:1885-92.
9) Keaveny TM, Donley DW, Hoffmann PF, Mitlak BH, Glass EV, San Martin JA. Effects of teriparatide and alendronate on vertebral strength as assessed by finite element modeling of QCT scans in women with osteoporosis. J Bone Miner Res 2007;22:149-57.
10) Boivin GY, Chavassieux PM, Santora AC, Yates J, Meunier PJ. Alendronate increases bone strength by increasing the mean degree of mineralization of bone tissue in osteoporotic women. Bone 2000;27:687-94.
11) Roschger P, Rinnerthaler S, Yates J, Rodan GA, Fratzl P, Klaushofer K. Alendronate increases degree and uniformity of mineralization in cancellous bone and decreases the porosity in cortical bone of osteoporotic women. Bone 2001;29:185-91.

Evaluation of Bone Strength Using Quantitative Computed Tomography Based Finite Element Method
- Clinical Application for the Diagnosis of Osteoporosis -

The Dept. of Orthopaedic Surgery, The University of Tokyo
Isao Ohnishi, Masahiko Bessho, Takuya Matsumoto, Masako Kaneko, Satoru Ohashi, Kazuhiro Imai, and Kozo Nakamura

The Computational Diagnostic Radiology and Preventive Medicine, The 22nd Century Medical Center, The University of Tokyo
Naoto Hayashi

The Dept. of Orthopaedic Surgery, Tokyo Metropolitan Geriatric Hospital
Fumiaki Tokimura

Tokyo Metropolitan Institute of Gerontology
Kim Hunkyung

Abstract

Fragility fractures are the most serious complication of osteoporosis and have been recognized as a major public health problem. It is essential to precisely quantify the strength of the fragile bone in order to estimate the fracture risk and plan preventive interventions. Quantitative computed tomography (QCT)-based finite element (FE) method (QCT/FEM) could possibly achieve precise assessment of the strength of the bone of interest. The purpose of the study was to create a simulation model that could accurately predict the strength and to apply this method in the wide range of clinical diagnosis in osteoporosis. We verified the accuracy of our model by load testing using fresh frozen cadaver specimens. The yield loads, fracture loads and principal strains of the prediction significantly correlated with those measured by load testing ($r=0.941$, 0.979, 0.963). FE analysis showed that the solid elements and shell elements in undergoing compressive failure were at the same region as the experimental fracture site.

QCT/FEM can predict vertebral compressive strength ex vivo. We aimed to assess vertebral fracture risk and alendronate effects on osteoporosis in vivo using QCT/FEM. Vertebral strength in 104 postmenopausal women was analyzed, and the discriminatory power for vertebral fracture was assessed cross-sectionally. Alendronate effects were also prospectively assessed in 33 patients with postmenopausal osteoporosis who were

treated with alendronate for 1 year. On the age and body weight adjusted logistic regression, vertebral strength had stronger discriminatory power for vertebral fracture (OR per SD change: 6.71) than areal bone mineral density (BMD) and volumetric BMD. The optimal point for the vertebral fracture threshold was 1.95 kN with 75.9% sensitivity and 78.7% specificity. At 3 months, vertebral strength significantly increased by 10.2% from baseline. The minimum principal strain distribution showed that the area of high fracture risk decreased. At 1 year, the density of the inner cancellous bone increased by 8.3%, while the density of the juxta-cortical area increased by 13.6%. QCT/FEM had higher discriminatory power for vertebral fracture than BMD and detected alendronate effects at 3 months. Alendronate altered density distributions, thereby decreasing the area with a high fracture risk, resulting in increased vertebral strength.

Prediction of proximal femur strength by a quantitative computed tomography-based finite element method -Creation of predicted strength data of the proximal femur according to age range in a normal population and analysis of risk factors for hip fracture-

*Kaneko, M; *Ohnishi, I; *Bessho, M;*Matsumoto, T; *Ohashi, S; *Tobita, K; *Nakamura, K
*Department of Orthopaedic Surgery, University of Tokyo, Tokyo, Japan.
email: ohnishii-dis@ h.u-tokyo.ac.jp

INTRODUCTION

Fall-related fragility fractures in elderly patients with osteoporosis, which can result in severe disability for activities of daily living, is one of the most serious diseases in modern society. However, only 44% of all non-vertebral fractures occur in women with a T-score below 2.5. In men, this percentage is even lower (21%) [1]. However, there is a clear need for the development of more sensitive risk assessment tools, using not only bone densitometry, but also other clinical predictors of fractures. Bone densitometries can explain 60-70% of bone strength and are limited in the ability to account for complex geometry, architecture, and heterogeneity of bone. However, quantitative computed tomography (QCT)-based finite element (FE) methods (QCT/FEM) are able to perform structural analyses taking these factors into consideration to accurately predict bone strength [2-3]. Some preliminary investigations into clinical applications of these methods have been reported [4-5]. To date, however, no basic data have been available regarding predicted strength (PS) by QCT/FEM with reference to age in a normal population. To apply this method for a wide range of clinical uses, a database of PS distributions with reference to age in a normal population is essential. The purpose of this study was thus to create a database on PS values of the proximal femur by QCT/FEM in a normal population as a preliminary trial. With these data, parameters that affect PS value by QCT/FEM were also analyzed.

Materials and Methods

Participants in this study comprised individuals who participated in a health checkup program with computed tomography (CT) at the University of Tokyo hospital from January to December in 2008 and for whom scan data were available for FEM subsequent analyses. The study protocol was approved by the ethics committee in our institution, and each participant provided written informed consent in accordance with the Declaration of Helsinki. Participants included 487 men (mean age, 55.0 years; range, 40-87 years) and 237 women (mean age, 59.0 years; range, 40-83 years). Exclusion criteria included patients with any recent or current disease under treatment with an agent to alter bone turnover or bone metabolism. In addition, subjects were excluded if they had any generalized disease that affects bone metabolism other than osteoporosis (e.g., hyperparathyroidism, hypo-parathyroidism, Paget's disease, renal osteodystrophy, Cushing's disease, steroid-induced osteoporosis, and others), malignant diseases, and rheumatoid arthritis. Scan data of the proximal femur were isolated and taken from overall data from CT of each participant with a slice thickness of 1.25 mm and a pixel width of 0.976 mm obtained using a Light Speed Ultra16 system (GE Yokokawa Medical System, Tokyo, Japan; 120 kV, 80 mAs, 512×512 matrix) with simultaneous scans of a calibration phantom (BMAS 200; Kyoto Kagaku, Kyoto, Japan) containing hydroxyapatite rods. A 3-dimensional FE model was constructed from the isolated data using Mechanical Finder software (RCCM, Tokyo, Japan). FE models were equipped with triangular shell elements with a thickness of 0.4 mm and a size of 3 mm for the outer surface of the cortical bone and tetrahedral solid elements with a size of 3 mm for the rest of the bone. We adopted two loading conditions, comprising stance and fall configurations [6]. Materially nonlinear FE analysis was performed using the Newton-Raphson method. Fracture load was defined as the load when at least one shell element failed. For each participant, height, weight, and abdominal circumference (AC) were measured, and medical history was elicited. Linear regression analysis was used to estimate correlations between age and PS of the proximal femur as analyzed by QCT/FEM. Change in PS with age was also evaluated by grouping participants into 5-year age brackets. One-way analysis of variance was used to compare average PS of participants in each age range. In addition, a multivariate statistical technique was used to determine how PS was affected by age, height, weight, and AC. The software SPSS（SPSS Inc, Chicago, USA）, was used for statistical analyses. Differences were considered significant for values of $p<0.05$. For highly correlated variables, variance inflation factor (VIF=1 /(1-R2)), which describes multi-collinearity, was computed. PS of the proximal femur was assigned to a dependent variable, while height, weight, age, and AC were assigned to independent variables. Multivariate statistical analyses were performed using stepwise method. In the analyses, when strongly correlated independent variables were included, they were excluded under a multi-collinearity of VIF≥5.

RESULTS

Average PS of the proximal femur in women was lower than that in men for each age range under both stance and fall loading configurations. PS under stance configuration in men showed a negative significant correlation with age ($p<0.05$), but no correlation with age was found under fall configuration ($p=0.678$). In women, PS showed a negative significant correlation with age under both stance and fall configurations ($p<0.05$). In men, average PS in the 75-79 year range was significantly lower than that in the <64 year range under stance configuration. In women, average PS at 40-44 years was significantly higher than that at >55 years under stance configuration, and was significantly higher than that at >65 years under fall configuration. In men, correlation between AC and weight was very strong with R=0.860. In addition, the VIF of AC was equal to 5.756 but the VIFs of other independent valuables were within a range of 1 to 2, so AC was excluded. In the multivariate analysis of PS in men under stance configuration, the standardized β for height was calculated as 0.045. Because height poorly correlated with PS with $p=0.348$, it was excluded from the analysis. Therefore, the multivariate analysis equation for PS in men under stance configuration was expressed with a standardized β for age of - 0.176 and that for weight of 0.386. Likewise, the multivariate analysis equation in men under fall configuration was expressed with a standardized β for weight of 0.201, that for height of 0.016 ($p=0.760$), and that for age of 0.031 ($p=0.490$). So, height and age correlated poor with PS, and they were excluded from the equation, which was finally expressed by a standardized β for weight of 0.212. In women, the correlation between AC and weight in women was also very strong with R=0.741 but the VIF for AC was equal to 1.874. Thus, both of these parameters could be included in the multivariate analysis equation. In the multivariate analysis of PS in women under stance configuration, the standardized β for height was calculated as 0.113 ($p=0.074$) and that for AC as 0.412 ($p=0.412$). Because height and AC poorly correlated with PS, they were excluded from the analysis equation. Therefore, the multivariate analysis equation for PS in women under stance configuration was expressed with a standardized β for age of - 0.444 and that for weight of 0.331. Likewise, the multivariate analysis equation in women under fall configuration was expressed with a standardized β for height of 0.104 ($p=0.124$) and that for AC of 0.071 ($p=0.944$). Because height and AC poorly correlated with PS, they were excluded from the analysis. Therefore, the multivariate analysis equation for PS in women under fall configuration was finally expressed with a standardized β for age of - 0.407 and that for weight of 0.209. Height did not significantly affect PS in either men or women.

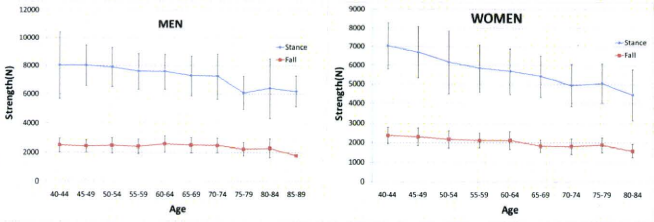

Figure 1: Change in PS of the proximal femur with age

DISCUSSION

This was the first study to investigate changes in PS of the proximal femur by QCT/FEM with age in a normal population. The number of participants in this study was small and may have been insufficient to suggest standard values for PS, but these results still contribute to creating basic standard data for PS in normal people in the future.

This study obtained the following results. First, average PS of the proximal femur was lower in women than in men for all age ranges. Second, PS in men under stance configuration, and those in women under both configurations significantly decreased with age. Third, weight positively affected PS in both men and women. Whether PS by QCT/FEM correlates more closely with fracture risk for osteoporotic patients in comparison to other bone densitometries remains unclear, but the present results did not contradict any existing concept of risk factors for fragility fracture. More baseline data for PS in normal populations need to be accumulated by increasing the number of participants in studies like this. In addition, more factors that affect PS should be analyzed to estimate risk factors for osteoporotic fracture.

REFERENCES:

1. Schuit, S.C., et al., Fracture incidence and association with bone mineral density in elderly men and women: the Rotterdam Study. Bone, 2004. 34(1): p. 195-202.
2. Keyak, J.H., et al., Prediction of femoral fracture load using automated finite element modeling. J Biomech, 1998. 31(2): p. 125-33.
3. Cody, D.D., et al., Femoral strength is better predicted by finite element models than QCT and DXA. J Biomech, 1999. 32(10): p. 1013-20.
4. Imai, K., et al., Assessment of vertebral fracture risk and therapeutic effects of alendronate in postmenopausal women using a quantitative computed tomography-based nonlinear finite element method. Osteoporos Int, 2009. 20(5): p. 801-10.
5. Orwoll, E.S., et al., Finite element analysis of the proximal femur and hip fracture risk in older men. J Bone Miner Res, 2009. 24(3): p. 475-83.
6. Bessho, M., et al., Prediction of strength and strain of the proximal femur by a CT-based finite element method. J Biomech, 2007. 40(8): p. 1745-53.

Strength index by quantitative computed tomography-based finite element method offers higher discriminatory power for hip fracture than areal bone mineral density of the femoral neck

+*Bessho, M; *Ohnishi, I; *Matsumoto, T; *Ohashi, S; *Kaneko, M; *Tobita, K; *Nakamura, K
+*Department of Orthopaedic Surgery, University of Tokyo, Tokyo, Japan
email: ohnishii-dis@ h.u-tokyo.ac.jp

Introduction: The increase in fragility fractures of the proximal femur has become a major problem in our aging society. Accurate assessment of fracture risk and establishment of effective prevention strategies are thus crucial for osteoporotic patients. We established a quantitative computed tomography (QCT)-based finite element (FE) method (QCT/FEM) that is able to more accurately quantify structural strength of the proximal femur compared to previous methods [1]. Previous experimental studies using mechanical testing of cadaver specimens disclosed that strength predicted by QCT/FEM correlated more closely with fracture load than the density value from dual energy X-ray absorptiometry (DXA) or QCT did [2]. However, no previous studies have evaluated the discriminatory power of QCT/FEM for hip fracture. The aim of this study was thus to compare the discriminatory power of QCT/FEM to that of areal bone mineral density (aBMD) and volumetric bone mineral density (vBMD) by conducting a cross-sectional case-control study with osteoporotic women with and without hip fracture.

Materials and Methods: Subjects comprised 41 women aged between 70 and 84 years old who completed a health examination in our institution from January 2008 to December 2008 (non-fracture group), and 30 patients aged between 70 and 84 years old with hip fracture (hip fracture group). Individuals with metallic implants within CT scan area were excluded. The 71 subjects had a mean age of 75.4 years (standard deviation (SD), 4.2 years), mean height of 150.4 cm (SD, 5.5 cm) and mean weight of 51.0 kg (SD, 7.8 kg). The study protocol was approved by our ethics committee and all subjects provided informed consent to participate prior to enrolment. For women without hip fracture, axial QCT was obtained for both the right proximal femur (Light Speed Ultra 16; GE Medical Yokokawa Medical Systems, Tokyo, Japan) (120 kV, 75 mAs, contiguous 2.5-mm thick slices, 512 × 512 matrices) and a calibration phantom (B-MAS200; Kyoto Kagaku, Kyoto, Japan). For patients with hip fracture, axial QCT was obtained for both the contralateral proximal femur (Aquilion Super 4; Toshiba Medical Systems, Tokyo, Japan) (120 kv, 75 mAs, contiguous 3.0-mm thick slices, 512 × 512 matrices) and a calibration phantom within 1 week after fracture. From the QCT data, FE models were created using triangular shell elements with a thickness of 0.4 mm and a size of 3 mm for the outer surface of the cortical bone and tetrahedral solid elements with a size of 3 mm for the rest of the bone [1]. To allow for bone heterogeneity, mechanical properties of each element were computed from the Hounsfield unit value. Ash density for each voxel was determined from the linear regression equation derived by relating the Hounsfield unit of a calibration phantom to the equivalent ash density. Young's modulus and yield stress of each tetrahedral element were calculated using the equations proposed by Keyak et al. [3] and Keller [4]. Poisson's ratio for each element was set as 0.4. Load and boundary conditions were applied to this model to represent two loading configurations, one approximating joint loading during single limb stance (stance configuration (SC)), and the other designed to simulate a fall on the greater trochanter (fall configuration (FC)) [3]. Materially nonlinear FE analysis was performed using the Newton-Raphson method. Predicted fracture load of the proximal femur was defined as the load causing failure at least one plate element [1]. Predicted fracture load was defined as proximal femoral strength index (PFSI). The same QCT scans were used to assess vBMD and aBMD of the proximal femur with commercially available software (QCT Pro; Mindways Software, Texas, USA), referring to the methods described by Bauer et al. [5]. For statistical analysis, the Mann-Whitney test was used to compare PFSI for SC, PFSI for FC, and aBMD and vBMD between groups. A receiver operating characteristics (ROC) curve was drawn to calculate area under the curve (AUC) for PFSI, aBMD and vBMD. Logistic regression analysis was performed to estimate risk factors for hip fracture. For each statistical analysis, differences were considered significant at $p<0.05$.

Results: Women in the non-fracture group had a mean age of 74.7 years (SD, 3.7 years), mean height of 151.2 cm (SD, 4.6 cm) and mean weight of 51.2 kg (SD, 8.0 kg). Patients with hip fracture had a mean age of 76.3 years (SD, 4.7 years), mean height of 149.3 cm (SD, 4.7 cm) and mean weight of 48.4 kg (SD, 7.3 kg). No significant differences in mean age, height or weight were apparent between groups ($p=0.10$, $p=0.14$ and $p=0.12$, respectively). Mean PFSI for the non-fracture group was 4950 N (SD, 1150 N) in SC and 1180 N (SD, 394 N) in FC. Mean PFSI for the fracture group was 3120 N (SD, 547 N) in SC and 980 N (SD, 247 N) in FC. Mean aBMDs for the non-fracture and fracture groups were 0.560 g/cm^2 (SD, 0.112 g/cm^2) and 0.429 g/cm^2 (SD, 0.086 g/cm^2), respectively. Mean vBMDs for the non-fracture and fracture groups were 260 g/cm^3 (SD, 60.4 g/cm^3) and 173 g/cm^3 (SD, 46.8 g/cm^3), respectively. Mean PFSI, aBMD and vBMD were significantly larger for the non-fracture group than for the fracture group ($p<0.0001$ each). The ROC curve is shown in Figure 1. AUCs for PFSI in SC, PFSI in FC, aBMD and vBMD were 0.943, 0.957, 0.836, and 0.879, respectively. AUC for PFSI in SC was not significantly different from that for PFSI in FC ($p=0.75$). AUCs for PFSI in SC and FC were significantly larger than that for aBMD ($p<0.012$, $p<0.005$). AUCs for PFSI in SC and FC were not significantly different from that for vBMD ($p=0.13$, $p=0.07$, respectively). Odds ratio associated with hip fracture per 0.5 SD change adjusted for age, height and weight was 12.0 (95% confidence interval (CI), 3.27-50.6, $p<0.001$) for PFSI in SC, 15.7 (95%CI, 3.20-77.4, $p<0.001$) for PFSI in FC, 2.21 (95%CI, 1.41-3.48, $p<0.001$) for aBMD, and 3.00 (95%CI, 1.72-5.22, $p<0.001$) for vBMD.

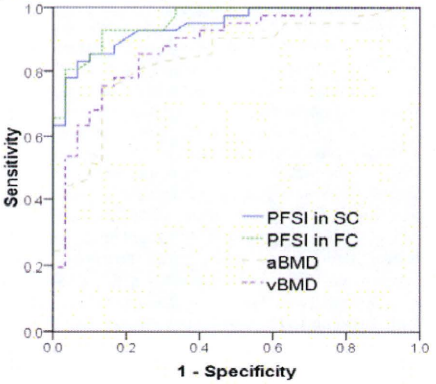

Figure 1: ROC curves showing 1-specificity (false-positive rate) vs. sensitivity (true positive rate) for the PFSI, aBMD and vBMD

Discussion: Risk of hip fracture is reportedly affected not only by decreased femoral neck BMD, but also by morphology of the proximal femur [6]. Evaluation of strength by QCT/FEM takes both BMD and morphology of the proximal femur into consideration, enabling 3-dimensional structural analysis. Strength prediction by QCT/FEM has been reported to accurately predict compressive strength of the proximal femur [2]. In the current investigation, strength index by QCT/FEM offered higher sensitivity and specificity for hip fracture discrimination than aBMD. Orwall et al. reported no significant differences in the discriminatory power for hip fracture between strength index by QCT/FEM and aBMD by DXA. The differences seen in our results may be due to differences in the FEM [7]. The current study was basically a cross-sectional case-control study, but a prospective cohort study will be necessary in the future to investigate the discriminatory power of strength index by QCT/FEM for hip fracture.

References: [1]Bessho, M. et al., J Biomech 2007;40: 1745-53. [2] Cody, D.D. et al., J Biomech 1999;32: 1013-20. [3] Keyak, J.H. et al., J Biomed Mater Res 1994;28: 1329-36. [4] Keller, T.S. J Biomech 1994;27: 1159-68. [5] Bauer, J.S. et al., AJR Am J Roentgenol 2007;188: 1294-301. [6] Faulkner, K.G. et al., J Bone Miner Res 1993;8: 1211-7. [7] Orwoll, E.S. et al., J Bone Miner Res 2009;24: 475-83.

Prediction of Vertebral Strength Under Loading Conditions of Daily Life Using a CT-Based Finite Element Method

+[1] Matsumoto, T; [1] Ohnishi, I; [1] Bessho, M; [1] Ohashi, S; [1]Kaneko, M; [1]Tobita, K; [1]Nakamura, K
+[1] *Department of Orthopaedic Surgery, University of Tokyo, Tokyo, Japan
taqmatsumoto@hotmail.com

INTRODUCTION: Osteoporotic vertebral fractures occasionally occur slowly and asymptomatically, that appear to be caused by loading on the spine during activities of daily living that exceed the vertebral strength of the osteoporotic individual. The most common type of vertebral fracture is reportedly wedge-shaped fracture caused by axial and bending loads. To assess the strength of osteoporotic vertebrae, evaluating vertebral strength under loading as experienced during daily living is important, particularly forward bending. The purpose of the present study was to evaluate differences in predicted fracture strength of vertebral bodies among different loading conditions occurring during activities of daily living using patient-specific finite element (FE) analysis (FEA), which provides accurate prediction of bone mechanics under loading reported by *Imai et al*

PATIENTS AND METHODS: Subjects comprised 41 female patients (mean age, 69.4 years; range, 51-88 years) with postmenopausal osteoporosis according to the guidelines for prevention and treatment of osteoporosis as proposed by the Japanese Society of Osteoporosis (2006 ed.). No subjects had any previous history of disease or use of drugs affecting bone metabolism. The second lumbar vertebra (L2) was examined in these patients, and subjects with previous L2 fracture were excluded. With ethics committee approval, computed tomography (CT) of L2 was performed after obtaining informed consent from each patient. CT of L2 was obtained using a slice thickness of 2 mm with a calibration phantom. CT data were transferred to the workstation, and bone area of the L2 vertebral body was extracted from each scan. FE mesh models were then generated using the advancing front method. An FE model was created with 2-mm tetrahedral elements. Triangular elements with a thickness of 0.4 mm were attached to the model surface. Mechanical Finder software was used to extract bone area and for FE analyses.To allow for bone heterogeneity, mechanical properties of each element were computed from the Hounsfield unit value. Ash density of each voxel was determined from the linear regression equation created by values from the calibration phantoms. Ash density of each element was set as the average ash density of voxels contained in one element. Young's modulus and yield stress of each tetrahedron element were calculated from the equations proposed by *Keyak et al (1998)*. The minimum Young's modulus of each triangular plate was set as 10 GPa. Poisson's ratio of each element was set at 0.4, as used in previous papers. A uniaxial compressive load with uniform distribution was applied on the upper surface of the vertebra, with all elements and all nodes of the lower surface completely restrained. Loading configurations for erect standing and forward bending as described by *Pollintine et al* (2004). were modified and adopted for analysis. Load distribution was divided into three parts: anterior; middle; and posterior. The ratio of load magnitude for each part was assigned on the assumption that the middle part bore the average load magnitude of the anterior and posterior parts. Ratios were thus 19:31:41 for erect standing and 59:48:38 for forward bending. Load was applied on the upper end plate vertically and the lower end plate was fully restrained (Fig. 1).

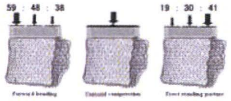

Figure 1: Load and boundary conditions in each model.

Nonlinear analysis was performed using the Newton-Raphson method with a post-yield modulus of 0.05. The ratio of ultimate stress to yield stress was assigned as 0.8. The element crack in tension was defined as occurring when maximum principal stress exceeded element ultimate stress. However, in compression, we introduced both yield and failure. Yield in compression was defined as occurring when Drucker-Prager equivalent stress exceeded element yield stress. Element failure in compression was then defined as occurring when the negative value of maximum principal strain exceeded 10,000 microstrain. Fracture load was defined as the load when at least one element failed. Predicted fracture load in each of the erect standing and forward bending configurations was calculated and compared to that under uniaxial compression. Predicted fracture sites under each loading configuration were also identified. To analyze differences in distribution of fracture sites depending on differences in loading configuration, the whole vertebral body was divided into 3 parts in an antero-posterior direction and 3 parts in a cranio-caudal direction, for a total of 9 parts. Pearson's correlation analyses were performed. Paired analyses among the three groups were performed using the Friedman multiple comparison test. Analysis of differences in distributions of predicted fracture sites was performed using the χ^2 test for all loading conditions. Deviation of the distribution was analyzed by Ryan's method. Differences were considered significant for values of $P<0.05$.

RESULTS: Mean fracture load was 3062 N under uniaxial compression (range, 883-5688 N), 2918 N in erect standing (range, 883-5492 N) and 2693 N in forward bending (range, 883-5296 N). The linear regression equation relating fracture load in erect standing to that under uniaxial compression was expressed as $y = 0.8912x + 19.332$ ($R=0.9522$, $P<0.0001$) (Fig. 2 a). Likewise, the equation relating forward bending to uniaxial compression was $y = 0.7033x + 55.071$, ($R=0.8342$, $P<0.0001$) (Fig. 2 b). Mean fracture load was significantly lower in forward bending than under uniaxial compression ($P=0.00017$).

Figure 2: a)Predicted strengths under uniaxial loading and erect standing. A significant correlation was identified. b) Predicted strengths under uniaxial loading and forward bending. A significant correlation was again identified.

The distribution of predicted fracture sites is shown in Figure 3 for each of the loading configurations. In the cranio-caudal direction, fracture sites tended to be located in the upper third of the vertebral body under all loading configurations. In the antero-posterior direction, the antero-superior part was the most frequent predicted fracture site in forward bending, with76% of all sites. For both erect standing and uniaxial compression, the middle-superior part was the most frequent site (Fig.3). Under all loading conditions, significant differences existed in the distribution of predicted fracture sites. Using Ryan's multiple comparison, the antero-superior part was the most frequent fracture site in forward bending ($P<0.005$).

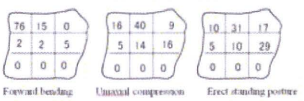

Figure 3: Distributions of predicted fracture sites under each of the loading configurations. Figures were expressed as percentages.

DISCUSSION: Fracture loads in erect standing and forward bending were highly correlated with those under uniaxial compression, however, the correlation between forward bending and uniaxial compression was moderate. Strength in forward bending was significantly lower than uniaxial compression according to Friedman analysis. Thus, when evaluating risk of vertebral fracture, assessment of predicted fracture load would need to be independently determined under each of the loading conditions to fully evaluate fracture risk during activities of daily living. Strength under uniaxial compression is clearly not representative of strengths under other loading configurations. If loading configurations under which the vertebrae are most vulnerable can be determined using CT based FE analysis, atraumatic osteoporotic fractures may be able to be prevented by instructing patients to avoid such postures in activities of daily living. In any case, assessment of fracture risk using a patient-specific CT-based FE method could contribute to preventing vertebral fracture by allowing instruction of patients with predicted high risk to avoid various risky postures during activities of daily living.

References: Imai, K., Spine, 2006, Keyak, J.H., et al. J Biomech, 1998, Pollintine, P., et al., Spine, 2004.

Effect of low-intensity pulsed ultrasound stimulation on gap healing in a rabbit osteotomy model evaluated by micro computed tomography-based 3-dimensional cross-sectional moment and cross-sectional moment of inertia

[1]Tobita, K; +[1]Ohnishi, I; [1]Matsumoto, T; [1]Ohashi, S; [1]Bessho, M; [1]Kaneko M; [1]Matsuyama, J; [1]Nakamura, K
+[1] Department of Orthopaedic Surgery, Faculty of Medicine, University of Tokyo, Tokyo, Japan
ohnishii-dis@h.u-tokyo.ac.jp

INTRODUCTION

Low-intensity pulsed ultrasound stimulation (LIPUS) reportedly enhances restoration of strength at fracture healing sites according to previous experimental studies [1]. However, evaluation of strength by mechanical testing is limited to only one direction, with either bending or torsion. Quantitative micro computed tomography (μCT) is able to acquire 3-dimensional (3D) histomorphometric data and density distributions of hard tissues, from which strength-related parameters can be calculated to allow strength analysis of the tissue. Strength-related parameters such as cross-sectional moment (CSM) and cross-sectional moment of inertia (CSMI) have been used to evaluate strength of the fracture healing site and reportedly correlate well with measured strength from mechanical testing [2]. However, previous studies have performed 2-dimensional (2D) analyses, and 3D evaluations have not been described. The purpose of this study was thus to investigate the effects of LIPUS on osteotomy healing using conducting 3D analyses of strength-related parameters of CSM and CSMI derived from μCT of the osteotomy gap.

MATERIALS AND METHODS

Surgical Procedures and LIPUS Treatment

A total of 42 skeletally mature between 21 and 23-week-old male Japanese white rabbits (Kitayama Labes, Nagano, Japan), weighing 3.4-4.0 kg, were used for this study. Under general anesthesia, four transfixation pins (diameter, 2 mm; length, 50 mm) were inserted at the metaphyseal regions of the tibia in the frontal plane using a custom-made surgical pin driver. Transverse osteotomy was performed using a T-saw (blade thickness, 0.36 mm) with continuous irrigation with saline solution across the mid-shaft of the tibia at 12 mm distal to the tibio-fibular junction. The osteotomy with a 2-mm gap was immobilized with four pins fixed to an external fixator with double side bars.

The LIPUS system (model SAFHS®2000J, Teijin Pharma, Tokyo, Japan), which transmits 200-μsec burst of 1-MHz sine waves repeated at 1kHz with an average intensity of 30mW/cm^2, was used. After postoperative day 3, LIPUS was continued under general anesthesia for both the treatment group (n=7/group/time point) and the control group (n=7/group/time point). The transducer was placed onto the anterior surface of the operated leg with ultrasound coupling gel, for 20 min, six times/week, for 4, 6, or 8 weeks. The control group also received a sham inactive transducer under exactly the same condition as the LIPUS group.

μCT Analysis

All animals were euthanized and the entire tibia was removed. The harvested tibia was scanned by μCT system (Scan X mate-E090, Comscantecno, Kanagawa, Japan). The scan was performed along the long axis of the diaphysis, with a voltage of 60 kVp and a current of 80 mA. Scan range covered 5 mm proximal and 5 mm distal to the center of the gap, with a resolution of 28.57 μm^3 voxel size. The region of interest (ROI) was set at the callus healing area (Fig. 1) defined by the gap filled with callus in 2D CT and extended 0.5 mm proximally and distally to the center of the osteotomy gap with a total of 36 CT axial scans. 3D reconstruction of mineralized tissue was performed using a TRI-BONE system (Ratoc System Engineering, Tokyo, Japan). A threshold for newly formed mineralized callus was set as 200 mg/cm^3. Morphometric parameters used for evaluation were mineralized callus volume (BV, cm^3) and mineralized callus contents (BMC, mg) calculated from the contoured ROI in 3D images, and volumetric bone mineral density of mineralized tissue comprising the callus (mBMD, mBMD = BMC/BV, mgHA/cm^3).

Center of gravity for the ROI was calculated automatically. The *Z* (polar) axis was defined to coincide with the long axis of the tibia. The *Y* axis was defined as parallel to the transfixation pins, which were also parallel to the posterior surface of the tibia (mediolateral (ML) direction). The *X* axis was defined as perpendicular to the *YZ* plane, and was directed anteroposterior (AP) on the tibia (Fig. 2).

Three-dimensional CSM and CSMI

An optional line (I) can be drawn in this *XYZ* coordinate. The angle of the *Z* axis (θ) was measured, and also the degree of angle of the *X* axis (φ) was measured (Fig. 3). The 3D CSM [I (φ, θ)] around this line was calculated as shown. 3D CSM was calculated using the following equation: $I(\varphi, \theta) = \int r^2 dV$ (mm^5), where r is the distance of a voxel to the center of gravity (mm) and dV (BV/voxel) is the area of a voxel (mm^3). The axial CSM was defined as CSMx: I (0, 90), CSMy: I (90, 90), whereas the polar CSM was also defined as CSMp: I (any, 0). We evaluated these three parameters as bone strength indices.

3D CSMI weighted by density distribution was calculated using the following equation: $I'(\varphi, \theta) = \int r^2 dm = \int \rho r^2 dV$ (mg·mm^2), where r is the distance of a voxel to the center of gravity, dm is the measured mineral content of a voxel in callus (BMC/voxel), ρ is the measured volumetric callus mineral density (mBMD), and dV (BV/voxel) is the area of a voxel (mm^3). CSMI x: I' (0, 90), CSMI y: I' (90, 90), and CSMI p: I' (any, 0) were calculated. These three parameters were evaluated as bone strength indices.

Statistical Analysis

The μCT evaluations were analyzed using a one-way ANOVA test. Data were all presented in mean and standard deviation (SD). Statistically significant difference was set at $p<0.05$.

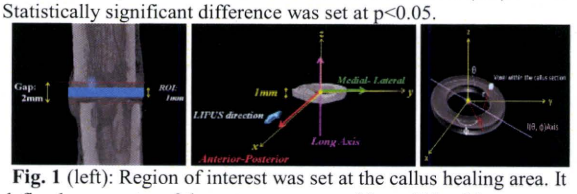

Fig. 1 (left): Region of interest was set at the callus healing area. It defined as a center of the osteotomy gap with a width of 1 mm.
Fig. 2 (middle): The *XYZ* plane was showed. The LIPUS transducer was placed onto the anterior surface of the operated leg
Fig. 3 (right): An optional line (I) can be drawn in this *XYZ* coordinate.

RESULTS

Three-dimensional CSM and CSMI

3D CSMs at the same time point were compared, values for the LIPUS groups were significantly higher than those for control groups for CSMx at 6 weeks ($p < 0.05$) and CSMp at 8 weeks ($p < 0.05$), Fig. 4A.

3D CSMIs at the same time point were compared, values for the LIPUS groups were significantly higher than those of the control groups for MOIx, MOIy, and MOIp at 6 and 8 weeks (Fig. 4B).

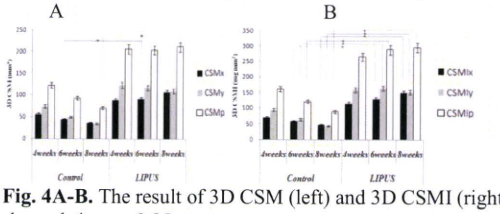

Fig. 4A-B. The result of 3D CSM (left) and 3D CSMI (right) were showed. *= $p < 0.05$.

DISCUSSION

CSM and CSMI are related to architectural strength and show bending and torsion properties. CSMI is a more reliable predictor than CSM for actual bone strength. CSMIp indicates torsional bone property, whereas the axial CSMIs of CSMIx and CSMIy indicate bending properties around the *X* and *Y* axes, respectively. We adopted 3D strength-related architectural parameters derived from μCT scans of the callus to evaluate the effects of LIPUS on restoration of mechanical integrity of the gap healing site.

Our results demonstrate that these bone strength parameters improved with LIPUS during the early phases. However, whether the late phase of callus formation is influenced remains unclear. The present study did not conduct mechanical testing, but μCT scans evaluated strength-related parameters in three independent planes. Mechanical testing can evaluate strength in only one plane for one specimen. Our results demonstrated that LIPUS improves initial restoration of strength at the healing site in bending in AP and ML planes, as well as torsion.

REFERENCES

1. Pilla AA et al, *J Orthop Trauma*, 1990
2. JL Ferretti et al, *J Musculoskel Neuron Interact*, 2001

ACKNOWLEDGEMENT

This project was supported by Teijin Pharma Limited, Tokyo, Japan.

Evaluation of the Accuracy of Articular Cartilage Thickness Measurement by Conventional and Real-time Spatial Compound Ultrasonography

[1]Ohashi, S; +[1]Ohnishi, I; [1]Matsumoto, [1]Bessho, T; [1]Matsuyama, J; M; [1]Tobita, K; [1]Kaneko M; [1]Nakamura, K
+[1] Department of Orthopaedic Surgery, Faculty of Medicine, University of Tokyo, Tokyo, Japan
ohnishii-dis@h.u-tokyo.ac.jp

INTRODUCTION

Articular cartilage thickness has previously been quantified by B-mode ultrasonography [1, 2]. However, cartilage surface and cartilage-bone borders have been decided manually in those studies. In addition, no studies have adopted real-time spatial compound ultrasonography for measuring cartilage thickness. The purpose of this study was to develop a method to objectively quantify articular cartilage thickness in vitro using both conventional and real-time spatial compound B-mode ultrasonography and to evaluate the accuracy of measurement.

MATERIALS AND METHODS

Cartilage samples

Knee joints were obtained for a 6-month- and a 3-year-old pig from a slaughterhouse (Tokyo Shibaura Zouki, Tokyo, Japan), as we assumed that thickness could differ between pigs at different ages. Femoral condyle articular cartilage was used in this study, since cartilage size and shape are relatively similar to those of human knee articular cartilage. After slaughter, whole bodies of pigs were kept at 3 °C in a refrigerated room. On the third day, the hind limbs were detached and sent to our laboratory under the same temperature. In our laboratory, limbs with intact knee joints were packed in plastic bags, degassed manually, sealed hermetically and stored at -20 °C. On the day of the experiment, soft tissues including joint capsules and ligaments were removed after the limbs were thawed in normal saline solution (Otsuka Pharmaceutical, Tokyo, Japan) at room temperature. Osteochondral blocks with the surface size of 20 × 20 mm from the medial femoral condyle were acquired by cutting the bone with a band saw (SWD-250; Fuijiwara Sangyo, Miki, Japan), then fixed on a custom-made acryl sample holder (30 × 30 × 13 mm; Murai & Co., Tokyo, Japan) with resin (GC-Ostron; GC Corporation, Tokyo, Japan). During preparation, samples were continuously cooled and moistened using normal saline solution.

Acoustic measurement

A B-mode 10.0-M Hz linear ultrasound probe (UST-5411; Aloka, Tokyo, Japan) connected to an ultrasound device (Prosound ALPHA 10; Aloka) was attached to a holding arm, which was fixed to a stage with an x,y micrometer for horizontal adjustment to enable identification of the location of cartilage measurement. In the water tank, osteochondral blocks and the transducer surface were placed in 20 °C water. The distance between transducer surfaces and the sample was kept as the transducer focus distance. Edges of the sample were identified by ultrasound signals, and the center of the sample was then identified from those points. B-mode images of the center line of the sample holder were acquired (Fig. 1A). Image settings were for both conventional imaging and real-time spatial compound imaging superimposed with three frames each from a different viewing angle of - 20, 0, and 20 degrees to the right angle. System settings were optimized for imaging the cartilage surface. Brightness line data of 32 points at 0.5-mm intervals in each image were obtained from both the 6-month- and 3-year-old pigs (Fig. 1B). The cartilage surface and cartilage-bone border of the specimen were defined as the peaks of each reflected signal. Cartilage thickness (Tc-US) was measured as the distance between peaks, which was adjusted by the ultrasound speed for each age from our past study [3].

Optical thickness measurement

The specimen fixed to the custom-made sample holder was mounted on a diamond saw device (Minitom; Struers, Westlake, OH), which offers an accuracy of 10 μm for adjustment of the cutting plane. A center-cut plane of the acryl sample holder was created, corresponding to the B-mode ultrasound image plane. Subsequently, each sample was mounted on a glass slide, covered with a cover glass after dripping normal saline onto the sample surface to keep the cartilage moistened and inhibit deformation during measurement due to drying. Cartilage thickness was measured using optical measuring microscopy (MM-400; Nikon, Tokyo, Japan). Using this optical measuring microscopy, points of line data acquisition on the cartilage surface and direction of the US beam were able to be identified from the position and orientation of the acryl sample holder surrounding the cartilage sample. Thickness of the cartilage (Tc) along the beam direction was measured at each point.

Mean and standard deviation (SD) of Tc for each sample were calculated. Linear regression analysis was performed and Pearson's coefficient of correlation was used to compare Tc-US to Tc. A correlation was considered significant for values of $p<0.05$.

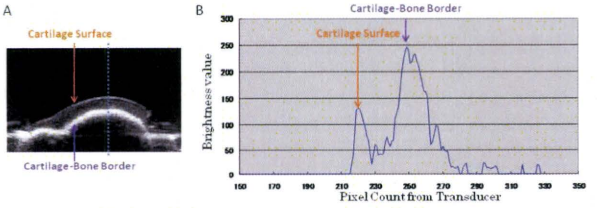

Figure 1: A) B-mode ultrasound image of the sample is shown. **B)** Line data acquired from the dotted line in the ultrasound image (A). Peak of the reflected ultrasound signal were defined as the surface and border of the tissue.

RESULTS

In all B-mode line data, peaks of reflected ultrasound signals from the cartilage surface and cartilage-bone border were clear enough to be identified. Mean Tc and Tc-US (conventional, spatial compound) for both samples are shown in Table 1. Tc-US was significantly correlated with Tc in both the 3-year- and 6-month-old pigs ($p<0.0001$ each) (Fig. 2). Pearson's coefficient of correlation tended to be slightly higher with spatial compound in each sample.

	6-month-old pig	3-year-old pig
Tc (mm)	2.40 ± 0.39	1.49 ± 0.10
Tc-US (conventional)	2.46 ± 0.42	1.45 ± 0.18
Tc-US (spatial compound)	2.40 ± 0.47	1.47 ± 0.14

Table 1. Mean Tc and Tc-US (mm). Values are provided as mean ±SD.

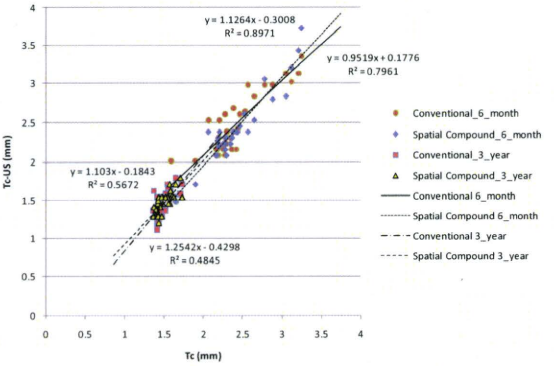

Figure 2. Scatter plot of each ultrasound image setting and sample. Linear regression analysis shows good agreement between Tc and Tc-US in all plots.

DISCUSSION

This is the first study to measure Tc using real-time spatial compound ultrasonography, which has been adopted in evaluating other tissues, such as tendon [4] and ligament [5]. From our results, real-time spatial compound ultrasonography may potentially have higher accuracy for measuring Tc than conventional methods, even though both showed good accuracy in our study. We believe the accuracy of our method is sufficiently high to allow application to measure human Tc in future studies.

REFERENCES:

[1] Myers et al. J Rheumatology, 1995; 22; 109-16.
[2] Burkhard et al. Arthritis & Rheumatism, 2009; 61; 435-41.
[3] Ohashi et al. 55th Orthopaedic Research Society, 2009.
[4] Bartolotta et al. Radiol Med. 2007 ; 112 ; 562-71.
[5] Sorrentino et al. Radiol Med. 2009 ; 114 ; 312-20.

ACKNOWLEDGEMENT:

This work was funded by the grant in aid of the Comprehensive Research on Aging and Health H19-007 of the Health and Labour Sciences Research Grants from the Ministry of Health, Labour and Welfare of Japan.

Title

Fracture reduction robot for safe and accurate fracture reduction of hip fracture.

Authors and Institution

Sanghyun Joung[1], Hongen Liao[1], Shinya Onogi[1], Mamoru Mitsuishi[1], Yoshikazu Nakajima[1], Nobuhiko Sugano[3], Masahiko Bessho[2], Satoru Ohashi[2], Takuya Matsumoto[2], Isao Ohnishi[2], Ichiro Sakuma[1]

[1]Graduate School of Engineering, the University of Tokyo, Japan,

[2]Graduate School of Medicine, the University of Tokyo, Japan,

[3]Graduate School of Medicine, Osaka University, Japan

Abstract

Hip fracture is a fracture in the proximal end of the femur. Most patients with hip fracture are treated operatively. In the case of displaced fractures, the fracture should be reduced before fixing the bone fragments. The first part of the procedure is the reduction of the fracture in the AP view by using longitudinal traction. Over distraction of the fracture must be avoided, as this may damage the femoral head vascularity. Next is the reduction in the lateral view by the internal rotation of the foot. Surgeons must exert a large force while pulling on the inferior branch and there are no safe methods available to avoid excessive force being put on the injured limb. This paper introduces a fracture reduction robot that has a high accuracy and reliable safety for assisting with hip fracture reduction.

The fracture reduction robot has six degrees of freedom (i.e, three DOFs in translation and three DOFs in rotation) of which precision are 1μmm in translation and 1μrad in rotation. For an accurate fracture reduction, the bone fragment is directly connected to the robot with the customized jig so that its position can be controlled precisely by the fracture reduction robot.

In order to limit the reduction force within the safe ranges, two mechanical failsafe modules are installed; one is for a traction direction and the other is for the internal or external rotation. The structure of two mechanical failsafe modules has a plunger style with a still-made roller pushed into a hollow by a spring. The threshold can be adjusted by changing the spring compression force. The software force limiter is also designed to prevent the excessive reduction force. Two thresholds are used not only to avoid the sudden stopping motion of the robot, but also to forewarn an operator of an increase in the reduction force by decelerating the robot. Two thresholds of the software force limiter are set smaller than the threshold force of the mechanical failsafe modules so that the mechanical failsafe is only operated when the software problem occurs.

The robot can rotate the bone fragment centering on one point of the bone fragment; this can reduce the movement of the soft tissues around the bone fragments. The algorithm is as follow: The method supposes that the force and moment given to the bone fragment by the surgeon is the movement direction intended by him. Then, the movement of each axis is calculated considering the bone fragment and the robot as a rigid body. One force sensor is installed to measure the force given to the bone fragment. The navigation system that has a function of 2D/3D registration will be used to determine the bones' coordinates.

The clinical usefulness of the safety features and the operation mode of the robot are evaluated with the simulated fracture reduction of a hip fracture model. Tests were conducted eight times. The reduction forces were recorded during the fracture reduction and the reduction results are evaluated from parameters related to the mechanical axis used to assess the femur deformity. The reduction force can be reduced within the set threshold of the software force limiter and the fracture model can be reduced within differences of 2 degrees and 2 mm comparing with the normal values. The fracture model could be accurately reduced with reliable safety.

Title

Force estimation acting on fixation screws for a safe direct fracture reduction.

Authors and Institution

Sanghyun Joung[1], Hongen Liao[1], Shinya Onogi[1], Mamoru Mitsuishi[1], Yoshikazu Nakajima[1], Nobuhiko Sugano[3], Masahiko Bessho[2], Satoru Ohashi[2], Takuya Matsumoto[2], Isao Ohnishi[2], Ichiro Sakuma[1]

[1]Graduate School of Engineering, the University of Tokyo, Japan,

[2]Graduate School of Medicine, the University of Tokyo, Japan,

[3]Graduate School of Medicine, Osaka University, Japan

Abstract

Most hip fractures are treated by operatively. With the displaced fracture, the fracture must be reduced before the fixation of the bone fragments. Surgeon handles an ankle in order to reduce the fracture. This is an invasive reduction method, but it is difficult to locate the bone fragments precisely. Thus, a direct reduction method is sometimes required for more accurate reduction in case of the complex fractures or a robot assisted fracture reduction. Two external fixation screws are inserted into the bone fragment in order to fix the bone fragment with a direct reduction method. And the two screws are connected to the handle like a ring or a half ring frame. With this method, the bone fragment may be damaged or a secondary fracture incurred by these screws subject to the weight of the patient's own leg and the resistive force against the reduction force. Therefore, it is important to monitor the force acting on a screw during the direct fracture reduction. This paper presents the estimation method of the pull-out and bending force acting on the fixation screws in real-time using the characteristic matrix, which expresses the material property, mechanical structure, the deformity, and more.

A force sensor of 6 degrees of freedom with handle is installed on the ring frame. However, due to the complex structure of the connection between the bone fragment and the fixation screws, the force distribution cannot be calculated easily using one force sensor. To solve the problem in real-time with a finite element analysis, it is assumed that the problem is linear, which means the outputs can be estimated from the previously calculated result. The method follows:

1. Two external fixation screws are inserted into the bone fragment.
2. The coordinates of the two screws and the force sensor are measured.
3. The coordinate information is input into the previously prepared CAD data that already have the material properties.
4. The characteristic matrix that defines the relation of inputs-force sensor- and outputs-force acting on two fixation screws-are calculated using the finite element analysis.
5. The applied forces to the screws are calculated in real time by multiply the measured force by the force sensor to the characteristic matrix during the fracture reduction.

The method is evaluated using a celluar rigid polyurethane foam block-density: 0.2g/cc- instead of the bone fragments. Two more force sensors are installed to measure the real force that is applied two fixation screws. The estimated forces by the proposed method and the measured forces by two additional force sensors are compared and correlations are calculated.

The evaluation results show the high correlation of pull-out force-0.87 at screw1 and 0.96 at screw2-, but the correlation of the resulting moments are low-0.65 at screw1 and 0.56 at screw2-. The simulation model used in this study has two limitations. First, the two fixation screws are fixed only at a point. The other thing is that the weight of the partial part is not considered. These cause a low correlation in the moment analysis. The resultants can be influenced by the loosened fixation of screws and the bone strength. It is, however, highly unlikely that the fracture is reduced with the loosened fixation of screws in clinical case. The influence of the weaken bone strength can be evaluated using the celluar rigid polyurethane foam that has a low density. To actually use the proposed method, the tight connection between the bone and the screw must be guaranteed, and a more precise analysis model is required; this is future work.

骨折整復支援ロボットの拘束動作の評価

○鄭常賢，廖洪恩，小林英津子，光石衛，中島義和，菅野伸彦[a]，別所雅彦，
大橋暁，大西五三男，佐久間一郎（東京大学，[a]大阪大学）

Evaluation of spatial constraint of a fracture reduction assisting robot

*Sanghyun JOUNG, Hongen LIAO, Kobayashi ETSUKO, Mamoru MITSUISHI,
Yoshikazu NAKAJIMA, Nobuhiko SUGANO[a], Masahiko BESSHO, Satoru OHASHI,
Isao OHNISHI, Ichiro SAKUMA, (the University of Tokyo, [a]Osaka University)

Abstract — We have developed a fracture reduction assisting robot for a hip fracture. A bone fragment is directly connected the robot using two external fixation screws for more precise positioning. We devised a manual control mode of the robot; which can assist in power and constrain a rotation center of the bone fragment. Movement of the rotation center was traced using the 3D optical measurement system. The resultants show that the proposed method has average error within 2mm though its maximum error is over 2mm. The error is mainly due to the play of the rotation axes of the robot. We will fix the mechanical fault and add in the more robust control method.

Key Words: Surgical robot, Fracture reduction, Spatial constraint, Power assistance

1. 背景

股関節骨折は大腿骨の骨盤側末端の骨折である．手術による治療が多く行われ，手術は折れた骨片を固定する前に骨片を元の位置に戻す骨折整復が行われる．従来の股関節骨折の整復は足首を持ち整復を行う介達式整復で，侵襲はないものの足首に与えられた整復力が関節，軟部組織に吸収され骨片の精確な位置操作が難しい．また，骨片の牽引は術者へ負担が大きく，牽引力を補助する牽引台が多く使用されるが，その自由度が足らず正確な整復は難しい．そこで，我々のグループでは整復力を補助しながら正確な整復を目指し，ロボット支援骨折整復に関する研究を進めている．これは，従来のように足首をもち整復を行う介達式整復をより正確に行うための研究と[1]，多少侵襲は発生するが，骨片に二つの創外固定ピンを挿入，そのピンをロボットと固定し，整復を行う直達式整復によるものがある．直達式では既にナビゲーションによるモデル骨の自動整復を行った[2]．術者がロボットを動かす手動モードに関してもその制御方法を発表したが[3]，その結果が要求仕様を満たしていなかった．また，ロボットの改良を行ったので報告する．

2. 方法

2.1 骨折整復支援ロボット

骨折整復支援システムは骨折整復支援ロボット(以下整復ロボット)とナビゲーションシステムに構成されている．ナビゲーションシステムは骨片間と整復ロボットとの位置関係を追跡し，骨片のゴール位置と整復パスを計算する．整復ロボットは骨片と繋がり正確に骨片を動かす役割をする．

図 1(a)に整復ロボットの外観を，図 1(b)にその動きを示す．ロボットは 6 自由度を持ち，そのうち 3 自由度は並進方向，3 自由度は回転方向である．牽引方向のボールスプライン構造にすることで撓みをなくし軽量化を図った．回転 3 軸は一点で交わる構造にして制御を簡便にした．

骨片と整復ロボットとの連結様子を図 2 に，その手順は以下に示す．まず，二つの創外固定ピンを挿入しリングフレームに固定する．整復ロボットには 6 自由度を持つ専用の固定ジグを取り付けリングフレームと繋げる．

骨折整復システムの臨床使用は 3 段階として考えている．先ずは，従来式の骨折整復にナビゲーションシステムの導入である．次は，整復ロボットの手動モードの導入であり，ナビゲーションシステム或いは放射線画像をみながら術者の操作による骨折整復である．最後にはナビゲーションシステムと整復ロボットとの統合による自動骨折整復方式を導

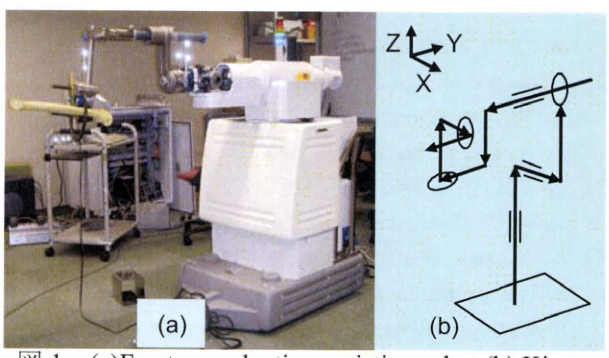

図 1. (a)Fracture reduction assisting robot (b) Kinematics of the robot

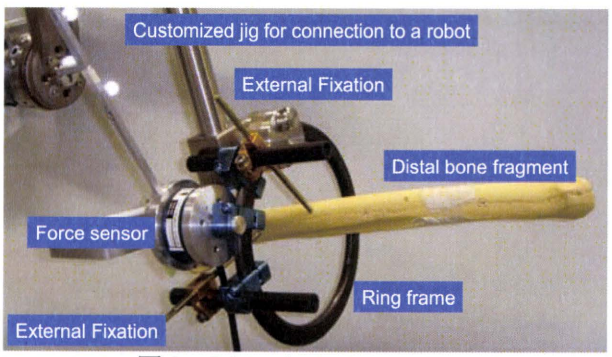

図 2. Direct bone connection

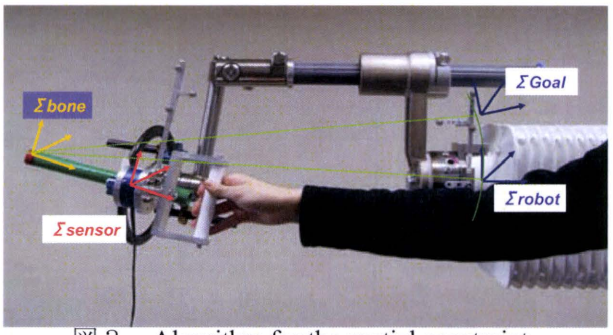

図３．Algorithm for the spatial constraint

入する．今回は整復ロボットによる手動整復に関して詳しく述べる．

2.2 整復ロボットによる手動整復

整復ロボットは整復力の補助だけではなく，骨片の動作空間を拘束する機能を実装した．これは，骨片の長軸に沿って骨片を牽引したり長軸周りに回旋させたりすることを可能とする．骨折面の一点を中心に骨片の回転させることは安全面でも重要なことであり，骨折部位の周辺組織の変位を減らす効果がある．

整復ロボットの制御方法を図に示す．術者は取っ手を持ち，骨片を動かす．取っ手とリングフレームの間には力センサがあり，術者が入れた力を計測する．力センサの入力値は骨片座標での力で変換する．そのとき，骨片座標系での力，モメント方向を術者が骨片を動かそうとした方向としてその大きさを変位量として仮定して骨片のゴール位置を計算する．骨片と整復ロボットを固体として考え，骨片のゴール位置から整復ロボットのゴール位置を計算する[3]．骨片座標の設定はナビゲーションシステムの2D/3Dレジストレーション方法を使用する見込みである[4]．

2.3 評価方法

光学式位置計測装置(Polaris,)を使い，骨片(Σbone)，力センサ(Σsensor)と整復ロボット(Σrobot)の座標を設定した．骨片座標の原点を中心に±15°程度回転しそのときの骨片座標の原点の位置を整復ロボット座標系で記録した．動作空間が正しく拘束されたら，骨片を動かしても骨片座標の原点は固定されるはずなので，最初の骨片座標の原点の位置からの変位を誤差として計算する．整復ロボットは直列構造であるため，軸の遊びなどが先端で大きく反映される．その影響を調べるため，整復ロボットを停止させた状態で先端を揺らしその動きを記録した．最後に計測装置の誤差を調べるために，整復ロボットの停止状態で骨片座標原点の位置の記録を行った．

3. 結果

評価結果を図に示す．横軸は制御誤差と整復ロボットのガタによる骨片原点の動きを整復ロボット座標系の各軸に分けたものである．縦軸には誤差の

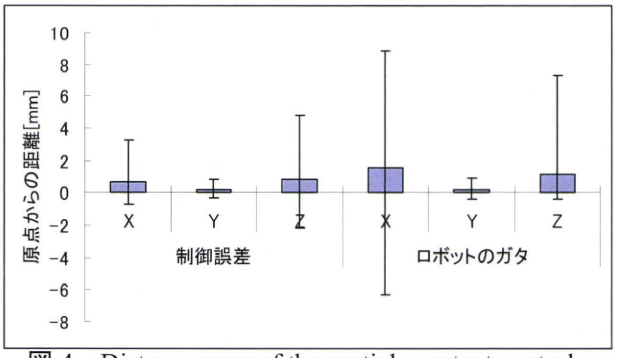

図 4. Distance error of the spatial constant control

平均と原点からの±最大距離を示す．光学式位置装置の誤差はX軸方向(計測機の奥行き方向)の誤差が多く，RMSで0.05mmであった．計測機のYとZ軸の誤差は何れも0.01mmであった．制御誤差，ガタによる動き共にX，Z軸が大きい変位を見せ，Z軸に関してはプラス方向(自重の反対方向)に偏っていることがわかる．

4. 考察と結論

骨折整復の整復力を支援するロボットを開発し，空間拘束が可能な制御方法を提案，評価した．整形外科では一般にあらゆる評価値が2mm, 2°以下であることが望ましい．空間拘束制御の結果，誤差の平均は2mm以下であったが，その最大値は2mmを超えている．誤差の原因は以下のように考えられる．

- 座標系を設定するときに生じる光学式位置計測装置の誤差によるもの．
- 整復ロボットの回転軸が持つガタによるもの．
- オープン制御を行ったことからのもの．

座標系設定による誤差は平均値を取ることにより小さく出来る．制御誤差がガタによる動きよりも小さいのは，整復ロボットを動かすために入れた力は20N程度であるが，最大のガタを発生するのに必要な力は60N程度であったためである．骨片座標の原点はロボット座標の原点から780mmはなれたところで位置したとこからX，Z軸のガタを見積るとX軸で1.4°，Z軸が0.5°である．今後整復ロボットの機械的問題を検討し，ロバスト制御を組み込む予定である．

参 考 文 献

[1] T. Douke et al.: “Control of Fracture Reduction Robot based on Biomechanical Model of Human Leg” , Bio-Rob2008, Arizona, USA, pp. 295-299, 2008

[2] S.Joung et al. : “A Robot Assisted Hip Fracture Reduction with a Navigation System”, Lecture Note in Computer Science 5242, pp.501-508, 2008

[3] 鄭常賢他: “直達式骨折整復用骨折整復支援システムの開発”, JSME annual meeting, pp.517-518, 2007

[4] Nakajima Y. et al.: “Parallel projected light field rendering and its application for intensity-based 2-D/3-D registration”, International Congress on Computer Assisted Radiology and Surgery (CARS) 2009, Berlin, Germany

直達式骨折整復支援システムの開発

○鄭常賢(ジョン　サンヒョン)　工学系研究科精密機械工学専攻
小林　英津子　工学系研究科精密機械工学専攻
中島　義和　工学系研究科バイオエンジニアリング専攻
光石　衛　工学系研究科産業機械工学専攻
大西　五三男　医学部整形外科
佐久間　一郎　工学系研究科精密機械工学専攻

高齢者に起こり易い大腿骨頚部骨折の治療法は外科的な手術によるものがほとんどである．手術では大腿骨の遠位骨片を牽引しながら整復し，ピンによって固定する．しかし，大腿筋などの周辺組織が萎縮した状態では整復のための牽引に大きな力が必要となるため術者にとって負担となる．また，X 線透視下で 2 次元の情報を用いて位置決めを行わなければならないため，術者の熟練が必要であり，手術を行うことで術者が受ける X 線被爆も問題である．

これらの問題に対し，我々は骨折整復支援システムを開発した．システムは骨折整復ロボットとナビゲーションシステムに構成されている．このシステムではロボットを使う利点を活かすため骨片にピンを打ち，ピンに連結されたリングを持って直接整復を行う直達式骨折整復方法を用いる．

骨折整復ロボットは並進 3 自由度と回転 3 自由度の 6 自由度を有する．骨片の牽引と回旋をするときの整復力が設定値より大きくなると各関連軸をフリーにするフェイルセイフ装置が装着されており安全性を保つ．ソフトウェアレベルでは整復力に対してロボットの速度を減らす手法で安全性を高める。動作モードは術者の整復力補助する手動モード，ナビゲーションからの指令により自動で整復を行う自動整復モードがある．

手動モードでは，骨片の大きな姿勢変化を防ぐため，骨片座標系でロボットを動かせるようにロボットの制御をする手法を提案しその精度評価を行った．

ナビゲーションシステムは術前に作成した CT からの 3 次元モデルを用いて整復ゴールを計算する．術中には C-arm で撮った画像と 3 次元モデルをレジストレーションすることにより，実空間での骨片間の位置関係を認知する．骨片の現在位置からゴールまでの整復パスは術者の意見を反映して作成され，整復ロボットに指令を送り整復を行う．開発したシステムにて骨折モデルでの整復実験を行い，その有効性を示す．

人体筋骨格モデルに基づく知的医療システムに関する研究

道家 健仁*, 中島 義和**, 小野木 真哉***, 杉田 直彦****, 光石 衛****, 別所 雅彦*****, 大橋 暁*****, 飛田 健治*****, 大西 五三男*****, 佐久間 一郎****, 土肥 健純****, 前田 ゆき******, 小山 毅******, 菅野 伸彦*******, 米延 策雄******, 松本 洋一郎****, 中村 耕三*****

*東京大学工学系研究科, 東京都文京区弥生 2-11-6
**東京大学工学系研究科, 東京大学 IML, 東京都文京区弥生 2-11-6
***東京大学 IML, 東京都文京区弥生 2-11-6
****東京大学工学系研究科, 東京都文京区本郷 7-3-1
*****東京大学医学系研究科, 東京都文京区本郷 7-3-1
******大阪南医療センター, 大阪府河内長野市木戸東町 2 番 1 号
*******大阪大学医学部, 大阪府吹田市山田丘 2-2

do@iml.u-tokyo.ac.jp

要旨

現状の大腿骨骨折整復手術は骨折部の状態を把握するために頻繁に術中 X 線撮影を行っており, 医師を始めとした医療スタッフおよび患者の X 線被曝量の低減が課題となっている. 本研究では, 骨折整復支援ロボットによる, より安全で精確な患者個々に適した整復動作手法の確立を目指す. 下肢の筋肉や靭帯をレオロジー物体とし, パラメータを持ったフォークトモデルを用いて下肢をモデル化した. 力と位置の測定値からパラメータの最適化を行い, 患者個々のパラメータ推定の可能性を検討した. 人体の筋肉・靭帯を模擬したゴムを人工骨に付着させた骨モデルを作製し, 牽引実験を行った. 計測は, ロボットの力センサによる力・トルク計測, 3次元位置計測装置による大腿骨と足先端の位置に関して行った. その結果, 推定値と実測値の誤差は力 7.8 N, トルク 0.078 Nm となり, 相関値は力が 0.97, トルクが 0.99 と非常に有意な相関を得た. 以上より提案手法による大腿骨位置姿勢推定の可能性が示された.

1. はじめに

近年, 患者側の立場に立った「優しい医療」が求められるようになってきている. その結果として患者の肉体的・精神的負担の軽減を目的とする低侵襲手術への志向が強くなり, 医療経済の面からみても, 効果的な医療が求められている. この低侵襲手術は, 大腿骨骨折整復手術にも普及してきている. 高齢化の影響もあり, 大腿骨骨折整復手術の需要が年々高まっている. しかし, 現状の大腿骨骨折整復手術には3つの課題がある. 1つ目は術中のレントゲン撮影により医師・患者ともに被曝してしまうこと, 2つ目は術者の体力的負担が大きいこと, 3つ目は2次元の CT 画像からでは整復計画が困難であることである. 特に, 医師ら医療スタッフは, 手術等で X 線被曝の機会が多く, その被曝量低減は重要な課題である. 現在, 骨折整復支援システム[1]の開発が行われており, この整復課題解決のために手術の自動化を目指している.

骨折整復支援システムで使用される骨折整復ロボットは, 患者の足の先端を把持し, 並進・回転をすることで牽引や回旋を任意に行うことが出来る. ロボットの足把持部には力センサが搭載されており, 足先端にかかる力・トルクが計測可能である. しかし, ロボットによる整復動作の際, 外力を加えるロボットと大腿骨骨片の間には足首関節や膝関節があるためロボットと大腿骨の移動量に差異が生まれ, 足把持部に加えた運動が必ずしもそのまま大腿骨骨片の運動にはならない. そのため, 大腿骨を目標とする位置へ移動させるためのロボットの制御法の確立は手術自動化への課題である.

本研究は, 大腿骨骨折整復における大腿骨位置姿勢に対する精確なロボット制御のために, 人体の生体特性[2][3]を考慮したロボットの制御法の確立を目指す.

2. 方法

2.1 大腿骨骨折整復システム

大腿骨骨折整復手術支援システムの構成は大きく分けて，手術ナビゲーションシステムと骨折整復ロボットの２つより構成される．手術ナビゲーションシステムは患者やシステム全体の状態を常に監視し，手術計画と手術シミュレーション，及び骨折整復ロボットへの動作指示を行う．骨折整復ロボットは，手術ナビゲーションシステムの計画・指示に従って実際の整復動作を行う．骨折整復ロボットを図１に示す．骨折整復ロボットは患者の足をブーツで把持し，患脚に対して実際の整復動作を行う．並進３軸，回転３軸の計６軸の駆動軸を有し，回転３軸は１点で交わるように設計されている．また，患者の足に加わる力を計測するために，ロボットは３軸の並進方向の力と３軸のトルクを計測できる力センサを備える．

図１　骨折整復ロボット

2.2 筋骨格モデルと生体パラメータの推定

本手法に利用できる情報は，大腿骨に取り付けたマーカによる大腿骨の位置姿勢と，ロボットによる足先の把持部の位置姿勢，ロボットが備える力センサの計測値である．解剖学の知見より，筋肉・靭帯をフォークトモデルで近似しモデルを構築した．筋肉は下肢の主動筋であり，大腿骨骨折整復に影響のある，大腿直筋・ハムストリング・大殿筋を選定し，靭帯は膝関節の靭帯である前十字靭帯・後十字靭帯・内側側副靭帯・外側側副靭帯を選定した．モデルの入力値には各筋肉・人体の長さが必要となる．各付着位置に関して，今回はファントムの実測値を用いたが，実際には標準統計形状モデルを適応させることで各個人に適切な付着位置を得る．回転角度，回転中心軸は計測したマーカの位置姿勢成分から算出する．

まず，各付着位置から靭帯・筋肉の単位方向ベクトルを算出する．

$$\overrightarrow{PQ_i} = \xi_i \vec{e}_x + \eta_i \vec{e}_y + \zeta_i \vec{e}_z \tag{3-1}$$

ここで，脛骨側の付着位置を P_i，大腿骨側の付着位置を Q_i とする．次に，靭帯・筋肉にかかる張力を求める．解剖学の知見より，靭帯・筋肉をバネ・ダンパで近似し，バネとダンパを平行に接続させたモデルを構築する．張力を $F_i(t)$，長さを $L_i(t)$，初期長を $L_i(0)$，バネ定数を k_i，ダンパ定数を c_i，時間を t とする．この時，張力 $F_i(t)$ は

$$F_i(t) = k_i(L_i(t) - L_i(0)) + c_i \frac{\partial L}{\partial t} \tag{3-2}$$

と表すことができる．これを牽引力とトルクに分解する．式(3-1)，(3-2)より牽引力 $F(t)$ は，

$$F(t) = \sum \eta_i \left(k_i(L_i(t) - L_i(0)) + c_i \frac{\partial L}{\partial t} \right) \tag{3-3}$$

となる．同様にトルク $T(t)$ は，

$$T(t)=\sum\left(\xi_i Pz_i-\zeta_i Px_i\right)\left(k_i(L_i(t)-L_i(0))+c_i\frac{\partial L}{\partial t}\right) \tag{3-4}$$

となる．

以上より，筋肉・靭帯の付着位置から長さを求め，足部にかかる力・トルクを算出することが出来る．靭帯・筋肉１つに対するパラメータを i 個，計測データを n 個とすると，１データから $2n$ 個の式が出力される．理論的には，データ数が n，筋肉・靭帯の生体組織数が i のとき，n が $1.5i$ 以上で方程式を解くことが出来る．実際には取得データ全てを用いた最小二乗法を用いた解の最適化を行い，パラメータの値を決定する．

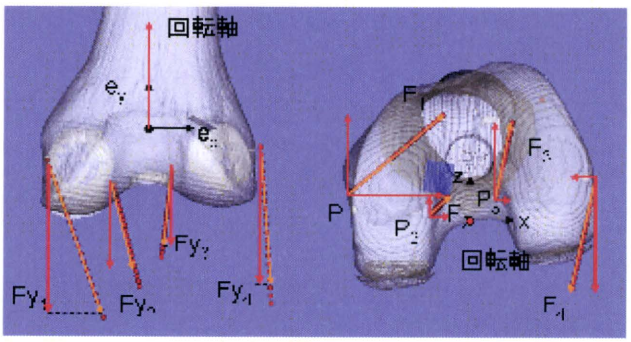

図３　力の分解

2.3　実験

実際に整復動作を行ったデータに対して提案手法が有用であるか検証を行った．実験にはプラスティック骨（SAWBONE，Pacific Research Laboratories，Inc.，USA）に筋肉・靭帯を模したゴムを貼り付けたファントムを使用した．計測はロボットの力センサによる力・トルク計測，３次元位置計測装置（OPTOTRAK™，Northern Digital Inc.，Canada）による大腿骨と足先端の位置計測を行い，牽引，回旋，牽引回旋の３種類の動作を行った．

3．結果

実験の結果を以下に述べる．回旋の結果を図５，図６に示す．力，トルクともに実測値に近い傾向を示した．推定値と実測値の誤差は力 7.8 N，トルク 0.078 Nm となった．牽引動作，牽引回旋動作では，力，トルクともに誤差が大きくなったが，推定値と実測値は同じ傾向を示し，相関値は力が 0.97，トルクが 0.99 と非常に有意な相関を得た．

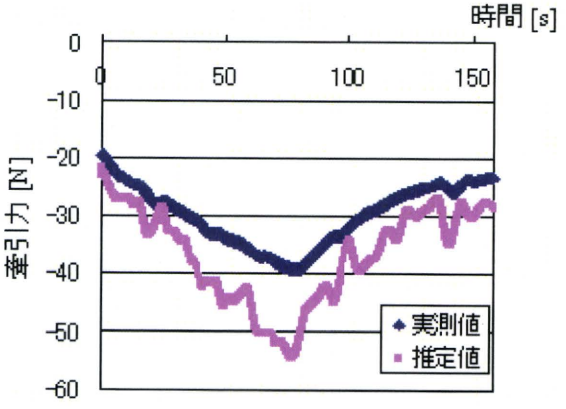

図５　回旋時の力の比較

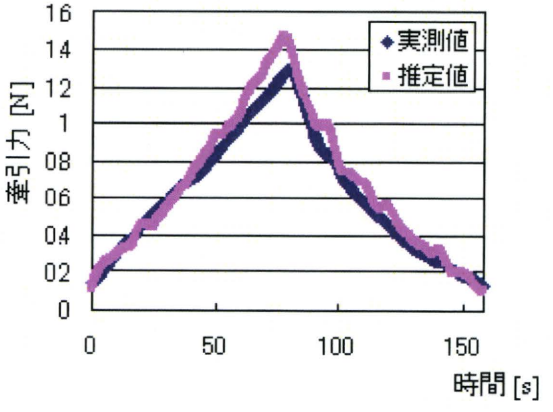

図６　回旋時のトルクの比較

4. 議論

結果から，力において実測値と推定値の誤差は大きくなったものの，力・トルク全体の傾向が一致したことから提案手法による大腿骨位置姿勢推定の可能性が示された．誤差の原因として，ファントムに取り付けた靭帯ゴムが構造上接着部のずれが生じてしまうことが考えられる．また，提案手法では生体組織は各付着部同士を直線で繋いでいる．しかし実際のファントムでは骨の形状によって靭帯，筋肉ゴムが骨に沿う形で屈曲している可能性があるため，推定した生体組織長さの違いが誤差に影響している可能性がある．よって今後，骨形状に沿う形でモデルを構築する必要がある．

5. おわりに

以上より，医学的知識に基づいた下肢の各関節の構造及び，生体物性を考慮した筋骨格モデルの構築を行った．その結果，提案手法による大腿骨位置姿勢推定の可能性が示され，骨折整復手術への適応可能性が示された．

参考文献

1. Y. Nakajima, et al., “Computer-assisted fracture reduction of proximal femur using preoperative CT data and intraoperative fluoroscopic images,” CARS 2004, Chicago, USA, 2004
2. Nihat Ozkaya, Margareta Nordin, “バイオメカニクス～生体力学の原理と応用,” NTS, 2001, pp. 250-252
3. N. Yamazaki, “Measurement and estimation of knee instability,” Society of Biomechanisms Japan, Biomechanisms, No. 9, pp. 115-125, 1988

第12巻第3号／2010年11月2日発行　　ISSN 1344-9486

Vol.12 No.3 2010

日本コンピュータ外科学会誌

Journal of Japan Society of Computer Aided Surgery

第19回日本コンピュータ外科学会大会特集号

Special Number / 19th Annual Congress of Japan Society of Computer Aided Surgery

会　期　2010年11月2日(火)・3日(水・祝)・4日(木)
会　場　九州大学医学部 百年講堂　　福岡市東区馬出3-1-1
大会長　橋爪 誠　九州大学大学院医学研究院 先端医療医学講座

■ 特別企画
特別講演／キーノートレクチャー
シンポジウム
1. 医療技術立国へ向けて～日本発の医療機器の実用化への課題
2. 医療機器におけるトランスレーショナル・リサーチの現状
パネルディスカッション
消化器・脳外科・耳鼻科・整形外科領域におけるCAS
第9回日本コンピュータ外科学会教育セミナー
ランチョンセミナー

■ 一般演題（口演／ポスター発表）
ロボット・マニピュレータ／内視鏡／脳神経外科／耳鼻科・頭頸部外科
セグメンテーション／ナビゲーション／VR・トレーニング・シミュレーション
消化器外科／胎児外科／整形外科／手術機器・デバイス／その他

協賛学会
精密工学会，日本医用画像工学会，日本医療機器学会，日本機械学会，日本生体医工学会，日本ロボット学会，ライフサポート学会

日本コンピュータ外科学会